Dust transport and deposition observed from the Terra-Moderate Resolution Imaging Spectroradiometer (MODIS) spacecraft over the Atlantic Ocean

Y. J. Kaufman,[1] I. Koren,[2,3] L. A. Remer,[1] D. Tanré,[4] P. Ginoux,[5] and S. Fan[5]

[1] Meteorological observations, in situ data, and satellite images of dust episodes were used already in the 1970s to estimate that 100 Tg of dust are transported from Africa over the Atlantic Ocean every year between June and August and are deposited in the Atlantic Ocean and the Americas. Desert dust is a main source of nutrients to oceanic biota and the Amazon forest, but it deteriorates air quality, as shown for Florida. Dust affects the Earth radiation budget, thus participating in climate change and feedback mechanisms. There is an urgent need for new tools for quantitative evaluation of the dust distribution, transport, and deposition. The Terra spacecraft, launched at the dawn of the last millennium, provides the first systematic well-calibrated multispectral measurements from the Moderate Resolution Imaging Spectroradiometer (MODIS) instrument for daily global analysis of aerosol. MODIS data are used here to distinguish dust from smoke and maritime aerosols and to evaluate the African dust column concentration, transport, and deposition. We found that 240 ± 80 Tg of dust are transported annually from Africa to the Atlantic Ocean, 140 ± 40 Tg are deposited in the Atlantic Ocean, 50 Tg fertilize the Amazon Basin (four times as previous estimates, thus explaining a paradox regarding the source of nutrition to the Amazon forest), 50 Tg reach the Caribbean, and 20 Tg return to Africa and Europe. The results are compared favorably with dust transport models for maximum particle diameter between 6 and 12 μm. This study is a first example of quantitative use of MODIS aerosol for a geophysical research.

1. Introduction

[2] *Prospero and Carlson* [1972], *Prospero and Nees* [1977] and *Carlson* [1979] used meteorological observations, in situ data and satellite images (AVHRR) of dust episodes, to derive the first estimates of dust emission from Africa of 100 Tg of dust for a latitude belt $5°–25°$N in the summer months June to August. This estimate was done before inaccuracies with AVHRR calibration were recognized and corrected [*Holben et al.*, 1990]. Owing to lack of systematic satellite measurements designed for aerosol studies, improvements in the estimates of dust emission were based mainly on models of the dust sources, emission and transport [*Tegen and Fung*, 1994; *Prospero et al.*, 1996;

Ginoux et al., 2001]. With the launch of the first Moderate Resolution Imaging Spectroradiometer (MODIS) instrument at the end of 1999, quantitative and systematic measurements of dust transport are possible [*Gao et al.*, 2001; *Kaufman et al.*, 2002] and presented here for the Atlantic ocean.

[3] The constant flux of dust across the Atlantic Ocean is of considerable interest. In the last 10 years the citation index reports 500 papers about or related to Saharan dust, and shows an exponential increase in the publication rate, starting from the early works of Prospero and Carlson in the 1970s (see Figure 1). Iron contained in aeolian dust was shown to be an important micronutrient for ocean phytoplankton, which could contribute to fluctuation of CO_2 on climatic timescales [*Martin et al.*, 1991] and contribute to climate variations. *Erickson et al.* [2003] measured, using satellite data, the effect of dust deposition on ocean productivity. Over the millennia, dust was suggested to be the main fertilizer of the Amazon forest [*Swap et al.*, 1992]. Desert dust, now considered to originate mainly from natural source [*Tegen et al.*, 2004] interact with solar and thermal radiation, thus can modulate the Earth radiation balance in response to changing climate conditions [*Prospero et al.*, 2002], i.e., changes in

[1]NASA Goddard Space Flight Center, Greenbelt, Maryland, USA.
[2]National Research Council, Greenbelt, Maryland, USA.
[3]Now at NASA Goddard Space Flight Center, Greenbelt, Maryland, USA.
[4]Laboratoire d'Optique Atmospherique, CNRS, Université de Science et Technique de Lille, Villeneuve d'Ascq, France.
[5]NOAA Geophysical Fluids Dynamics Laboratory, Princeton University, Princeton, New Jersey, USA.
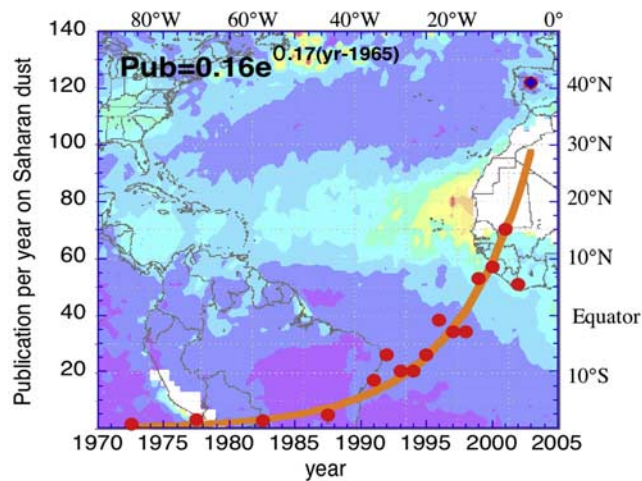
Figure 1. Back to African dust: Exponential publication rate on Saharan dust (red dots) according to the ISI citation index, on a background of MODIS aerosol optical thickness for July 2001. The exponential growth corresponds to doubling of the publication rate every 4 years, as compared to publication rate on climate change that doubles every 11 years [*Stanhill*, 2001]. The publication search was performed under the term "dust and Sahar*" and is conducted on the title, abstract, and keywords. Note that the ISI "keywords plus" introduces additional keywords that generate, in this case, 10–20% of unrelated citations and cannot be excluded from the search.

precipitation in the Soudano-Sahel region [*Prospero and Lamb*, 2003]. Dust particles can also interact with clouds, mainly after absorbing hygroscopic material [*Levin et al.*, 1996; *Rosenfeld et al.*, 2001].

[4] The emission of dust is associated with strong winds, generating optical thicknesses as high as 3.5 [*Pinker et al.*, 2001] in pulses of dust, each several days long [*Carlson*, 1979]. Dust also affects photolysis rates and heterogeneous reactions for ozone chemistry, by changing the concentration of UV radiation [*Dentener et al.*, 1996; *Martin et al.*, 2003].

[5] The MODIS systematic and accurate measurements of aerosol optical thickness (τ) and the contribution to the optical thickness by the fine mode (f) [*Tanré et al.*, 1997; *King et al.*, 1999, 2003] can be used to derive the dust column concentration, flux and deposition in the Atlantic Ocean. Here we implement an approach to distinguish dust from other aerosol types using the MODIS measurements and use it to derive dust transport and deposition. This is one of the first examples of quantitative use of MODIS aerosol data for geophysical studies.

2. Aerosol Measurements From Satellites

[6] Since the early observations of African dust from the AVHRR [*Carlson*, 1979], the AVHRR was used to observe the seasonal and interannual variability of dust emissions [*Swap et al.*, 1992, 1996; *Husar et al.*, 1997; *Cakmur et al.*, 2001]. AVHRR data were used to estimate that 100 Tg of dust leave Africa annually in the summer toward the Caribbean and Florida [*Carlson*, 1979] and that in the winter out of the 30 Tg of dust that cross the 60°W line,

13 Tg arrive to the Amazon Basin and are deposited by rain [*Swap et al.*, 1992]. This analysis of the AVHRR data allowed *Swap et al.* [1992] to suggest that recycling of nutrients in the biologically rich Amazon Basin over thousands of years timescales depends on dust transport and deposition from the African Soudano-Sahel and Saharan regions. However, they pointed out that 50 Tg are needed to keep the Amazon fertilized, creating a paradox of the missing nutrients.

[7] Despite these insights gained from the AVHRR, a spaceborne sensor not designed originally for aerosol measurements, the accuracy of the AVHRR data regarding aerosol is limited. AVHRR was not used to distinguish between dust, smoke, pollution, stratospheric aerosol or sea salt, therefore the interpretation of aerosol measurements as dust depends on outside knowledge of the aerosol type and composition that is often incomplete. For example *Swap et al.* [1996] found differences of factor of 3 in dust deposition between the end of the 1980s and the beginning of the 1990s, attributing it to dust, despite the presence of heavy stratospheric aerosol in 1991 and 1992 from the Pinatubo eruption. Analysis of the AVHRR data created therefore the impression that maximum dust transport from Africa occurs in February [*Swap et al.*, 1996], while here we show that the maximum is in the summer, as suggested already by Carlson and Prospero in the 1970s. This misinterpretation of seasonality stems from considering the mixture of smoke from the Sahel with dust from the Sahara in February as pure dust. In June–July biomass burning moves south and is not mixed with dust emitted from the Sahara. Only recently the AVHRR aerosol data became better calibrated and validated [*Ignatov and Stowe*, 2002]. Note that *Prospero et al.* [1981] did find higher dust concentration in the boreal summer months using in situ measurements at surface level.

[8] TOMS UV measurements were found to be sensitive to dust and smoke due to their absorption of sunlight reflected in the UV by atmospheric gases [*Hsu et al.*, 1996; *Herman et al.*, 1997]. TOMS can distinguish between the absorbing dust and smoke aerosol from pollution and sea salt that do not absorb sunlight [*Torres et al.*, 2002]. TOMS data were used to identify globally the location and geomorphological characteristics of dust sources [*Prospero et al.*, 2002], their physical and optical characteristics [*Ginoux and Torres*, 2003], and to verify the location of dust sources estimated in the model using an independent scheme [*Ginoux et al.*, 2001]. The African dust sources were found to be located in sparsely populated areas, north of 15°N, where the human influence on the dust sources is very limited [*Prospero et al.*, 2002]. Together with the Aerosol Robotic Network (AERONET) of Sun sky radiometers TOMS data were used to test and improve dust emission and transport models [*Chin et al.*, 2002; *Ginoux et al.*, 2003], and to initialize dust transport models [*Alpert et al.*, 2002].

[9] Several authors used TOMS aerosol index to investigate the variability of dust distribution on a seasonal [*Cakmur et al.*, 2001] and interannual [*Chiapello and Moulin*, 2002; *Ginoux et al.*, 2003] scales. *Cakmur et al.* [2001] showed the seasonal cycle using TOMS and AVHRR, with maximum dust concentrations in the summer, and explained the much sharper annual cycle observed by
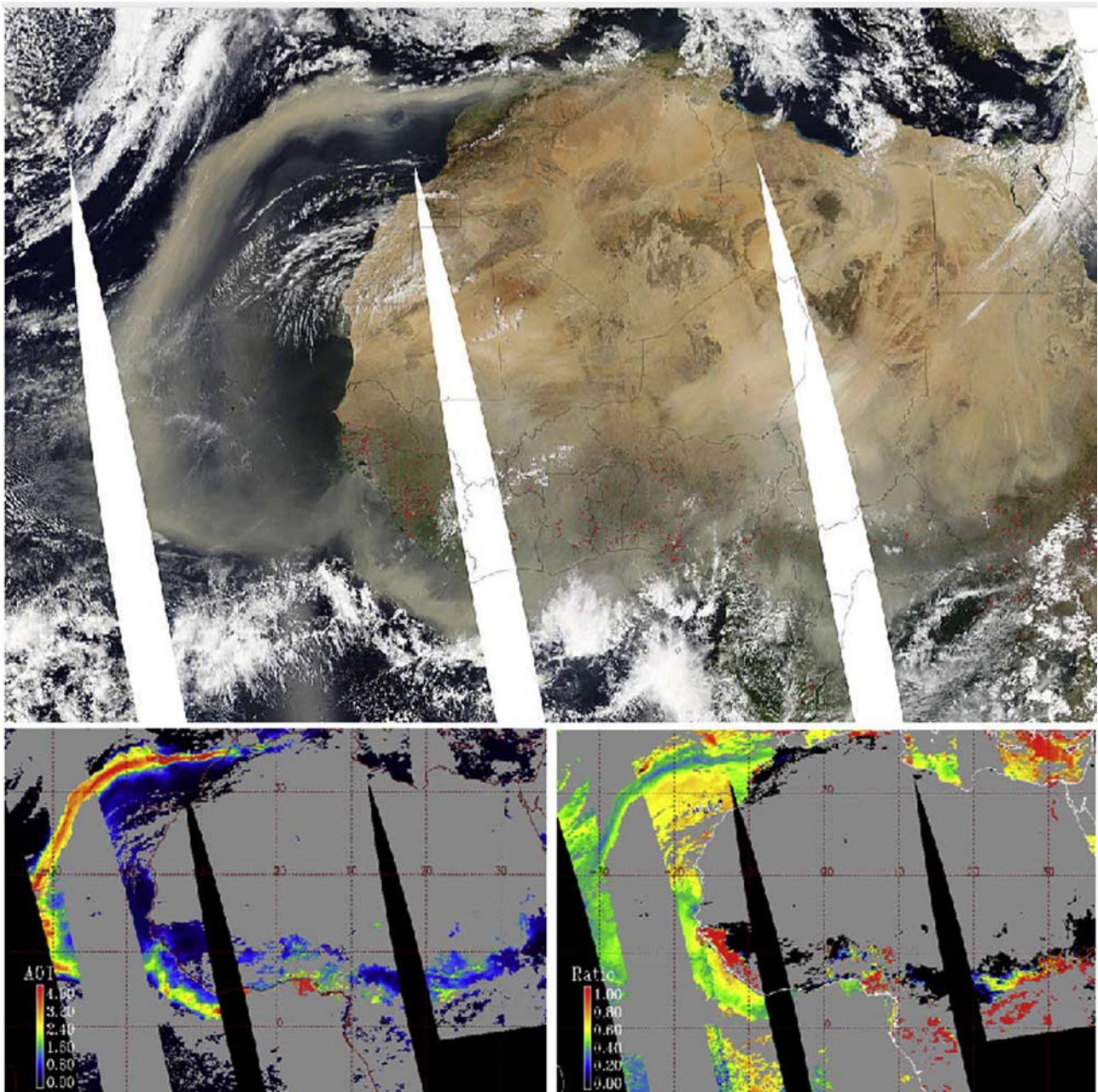
Figure 2. (top) MODIS color composite of dust storm (sand color) emerging to the Atlantic Ocean south of the Sahara and circulating in the Atlantic ocean back to northern Africa (taken from http://rapidfire.sci.gsfc.nasa.gov/gallery). Note that fires (red dots) in the south emit smoke into the dusty atmosphere. The image was taken from the Aqua satellite on 6 March 2004. The two lower panels show (left) analysis of the optical thickness of the dust, smoke, and background aerosol. The gray areas are regions where land or ocean glint are too bright to be used to derive the aerosol properties. (right) The fraction of the optical thickness due to fine (less than 1 micron diameter) aerosol particles. Blue-green colors, fraction of 0.4–0.5 represents dust; orange-red colors, fraction of 0.7–1.0 represents mixed in smoke.

TOMS than by AVHRR by the variation of the dust altitude (close to the surface in the winter months; *Chiapello et al.* [1995]). TOMS measurements are sensitive to the height of the aerosol, as well as to their concentration.

[10] *Chiapello et al.* [1999] compared TOMS aerosol index with ground based measurements, showing excellent agreement in Barbados and lesser agreement in Capo-Verde, where the seasonal variation of the vertical distribution causes high dust concentration near the surface in the winter months, while in the summer the dust flows above the area [*Karyampudi et al.*, 1999] on its way to Barbados, as was shown from Meteosat by *Jankowiak and Tanré* [1992]. The variation in spatial, seasonal and interannual dust concentration observed from *Meteosat* [*Jankowiak and Tanré*, 1992], generated interest in the origin of this variation, e.g., correlation with the North Atlantic oscillations [*Moulin*
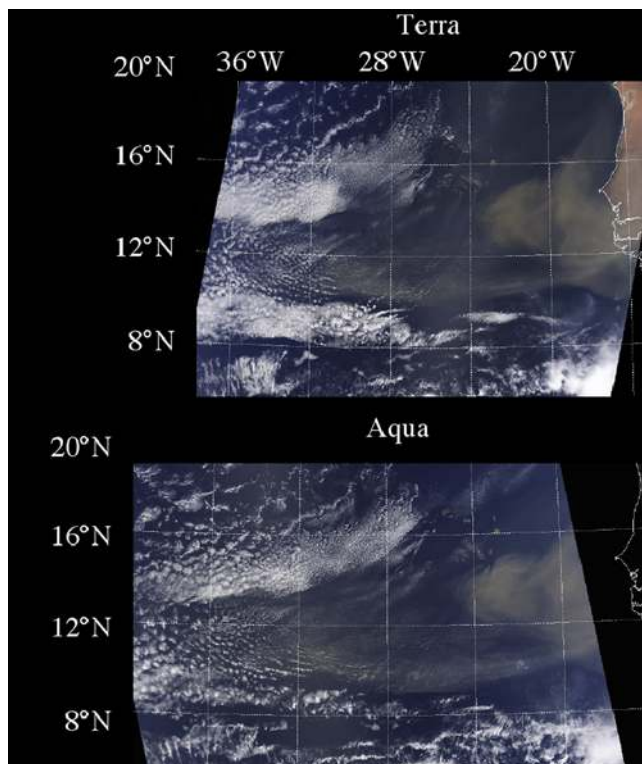
Figure 3. Examples of MODIS observation of dust storms off the coast of Africa for Terra (1030 LT) and Aqua (1330 LT) for 1 May 2003. The image is a composite of visible channels (0.47, 0.55, and 0.66 μm for the blue green and red colors). The dust storm moved 120 km between the Terra and Aqua observations, corresponding to wind speed in the dust layer of 11 m/s.

et al., 1997a] and in its use to measure the climatic temperature response to the presence of dust [Alpert et al., 1998]. Conversion of the AVHRR, TOMS or METEOSAT data to dust column loading depends on the quality of calibration, and validity of assumptions on the aerosol scattering properties and height in the case of TOMS.

[11] Measurements from the MODIS instruments provide new opportunities. MODIS began collecting data in April 2000 and May 2002 from Terra and Aqua spacecraft respectively. Special emphasis is given to onboard calibration facilities, lunar observations and detailed analysis of the calibration time series on the ground [Barnes et al., 1998]. MODIS measured spectral radiances from 0.47 μm to 2.1 μm are used to characterize the global aerosol. The aerosol characteristics are derived over the oceans [Tanré et al., 1997] and land [Kaufman et al., 1997] using independent algorithms. In this paper we use only the ocean data. Over the oceans, the MODIS aerosol algorithm uses the measured 500 m resolution radiance from six MODIS bands (550–2100 nm) to retrieve the aerosol information. In order to screen for clouds [Martins et al., 2002], and generate a statistically robust aerosol measurement, the analysis is performed on a grid box of 10 km at the subsatellite point. The average of the measured spectral radiance over cloud-free, glint-free ocean scenes, is used to derive the aerosol information by fitting it to a lookup table, that includes both fine aerosol (effective radius between

0.1, and 0.25 μm) and coarse aerosol (effective radius between 1 and 2.5 μm). In the process, the best fitting fine and coarse models are chosen and the optical thickness at 550 nm, τ, and the fraction of τ contributed by the fine aerosol, f, are determined [Tanré et al., 1997]. Aggregation of the MODIS aerosol information from the 500 m pixels to the 10 km product, allows rigorous cloud screening, avoiding data gaps and still generates large enough statistics for a stable and accurate product. The MODIS derived aerosol optical thicknesses were validated before [Tanré et al., 1999] and after [Remer et al., 2002] the launch of Terra. In agreement with theoretical error analysis [Tanré et al., 1997], the aerosol optical thickness is derived with an error of $\Delta\tau \pm 0.03 \pm 0.05\tau$, against AERONET data. The errors were found to be mostly random with very little bias remaining for large statistics of data [Remer et al., 2002]. For aerosol dominated by dust a bias of about +5% was noticed. The fine mode fraction, f, is defined as the fraction of the total optical thickness attributed to the selected fine mode. Its uncertainty is estimated to be ±0.2 [Tanré et al., 1996, 1997; R. Kleidman et al., manuscript in preparation, 2004]. Figure 2 shows an example of the MODIS observations of a dust storm off the coast of Africa and analysis of the optical thickness and fine aerosol fraction. The analysis distinguishes clouds from aerosol. The fine fraction image shows the dust plume (green to blue) and mixed in smoke (orange to red) from fires in the southern part of the image. Figure 3 shows dust progression observations from Terra and Aqua, and Figure 4 the monthly variation of dust and smoke over the Atlantic Ocean.

3. Dust Column Concentration

[12] The dust column concentration is calculated using MODIS measurements of the aerosol optical thickness, τ at 550 nm, and the fraction of τ contributed by the fine aerosol, f. Note that the meaning of the fraction f is that the optical thickness of the fine aerosol is: $f\tau$, and of the coarse aerosol: $(1-f)\tau$. The fraction f is used to distinguish dust from biomass burning aerosol [Kaufman et al., 2002] as described below. The aerosol optical thickness measured by MODIS is composed of maritime, τ_{ma}, dust, τ_{du}, and anthropogenic, τ_{an}, aerosol (biomass burning and urban industrial pollution):

$$\tau = \tau_{ma} + \tau_{du} + \tau_{an}. \qquad (1)$$

We do not have a mechanism to distinguish dust from maritime aerosol in the MODIS data, therefore we estimate the maritime aerosol optical thickness independently of the MODIS measurements. In remote areas, with little contamination of the maritime atmosphere we found that on average $\tau_{ma} = 0.06 \pm 0.005$, in agreement with an analysis of baseline maritime aerosol [Kaufman et al., 2001] and with the analysis of natural aerosol in INDOEX of $\tau_{ma} = 0.07$ [Ramanathan et al., 2001]. This information is combined with wind-dependent measurements of aerosol optical thickness in Midway island [Smirnov et al., 2003] of:

$$\tau_{ma} = 0.007W(m/s) + 0.05, \qquad (2)$$

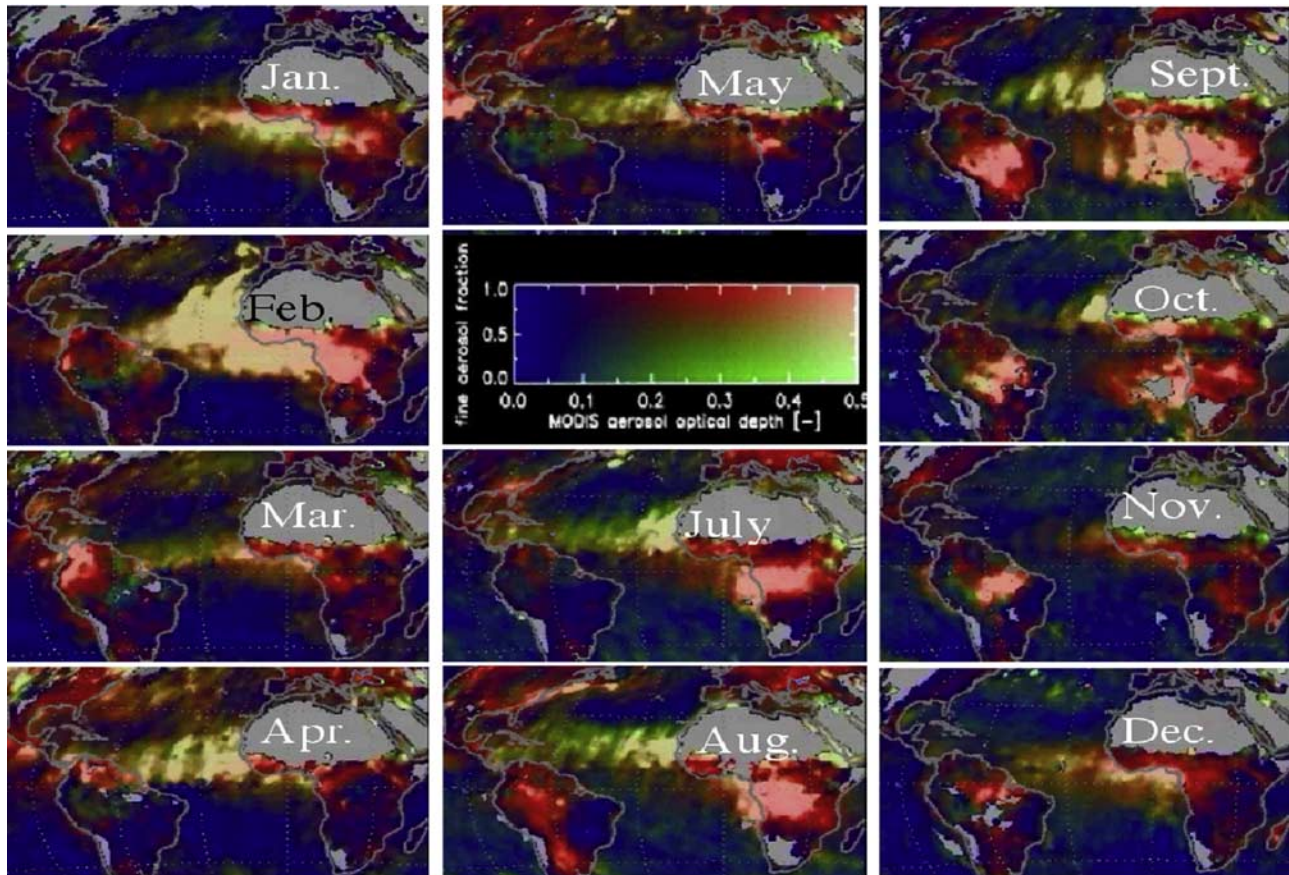where W is the wind speed and the optical thickness was interpolated to 550 nm. Since in Midway the aerosol can

Figure 4. MODIS aerosol monthly composites for 2001 taken from a movie at http://earthobservatory.nasa.gov/Newsroom/Aerosols/. Each composite is for the 15th of each month ±5 days to find enough cloud free regions. Data for June are not shown since no MODIS data were available during the middle of the month. The color bar is located instead. The color bar was constructed so that blue represents clean conditions, aerosol optical thickness <0.1, and green and red show higher optical thickness corresponding to the coarse (green) and fine (red) modes. The fine fraction (y axis) varies from green for fine fraction of zero to red for fine fraction of 1. Therefore pure dust is green, and pure smoke or pollution is red. Note that the color of the aerosol emitted from Africa changes from mixed red and green in January–April to green in July–August. Biomass burning occurs in the Sahel during January–March and moves to southern Africa for July–August, when it is separated from the dust flow.

contain nonmaritime elements, we reduce the offset in equation (2) to 0.02, to fit the average baseline aerosol optical thickness of 0.06 for the typical wind speed of 6 m/s. Therefore

$$\tau_{ma} = 0.007W + 0.02. \qquad (2')$$

[13] The NCEP reanalysis data set is used to calculate the surface winds (1000 mb) for equation (2). Fine aerosol is found in different proportions in the maritime aerosol, dust or anthropogenic aerosol. *Kaufman et al.* [2002] suggested that the much higher fraction of fine particles in anthropogenic aerosol as compared to dust or maritime aerosol can be used to distinguish between them in regions with high anthropogenic or dust concentrations. The procedure to do so follows:

[14] The contribution of the fine aerosol to the optical thickness for a mixture of dust, maritime aerosol and anthropogenic aerosol is:

$$f = [f_{ma}\tau_{ma} + f_{du}\tau_{du} + f_{an}\tau_{an}]/\tau, \qquad (3)$$

where f_{ma}, f_{du} and f_{an} are the fine mode fraction that correspond to the maritime, dust and anthropogenic aerosol respectively.

[15] Equation (3) can be used to deduce the dust optical thickness, τ_{du}:

$$\tau_{du} = [\tau(f_{an} - f) - \tau_{ma}(f_{an} - f_{ma})]/(f_{an} - f_{du}), \qquad (4)$$

where f is bounded by: $f_{an} \geq f \geq \min\{f_{an}, f_{du}\}$. Any value outside these bounds is set to the limit values: $f = f_{an}$ for $f > f_{an}$ and $\min\{f_{an}, f_{du}\}$ for $f < \min\{f_{an}, f_{du}\}$.

[16] To derive the fraction of the optical thickness due to the dust, we determine the fraction of fine aerosol for each of these aerosol types using MODIS aerosol measurements in regions of: concentrated dust, concentrated smoke, and mostly maritime aerosol in the southern Atlantic (0–30°S). The results are:

$$f_{ma} = 0.3 \pm 0.1, f_{du} = 0.5 \pm 0.05 \text{ and } f_{an} = 0.9 \pm 0.05. \qquad (5)$$
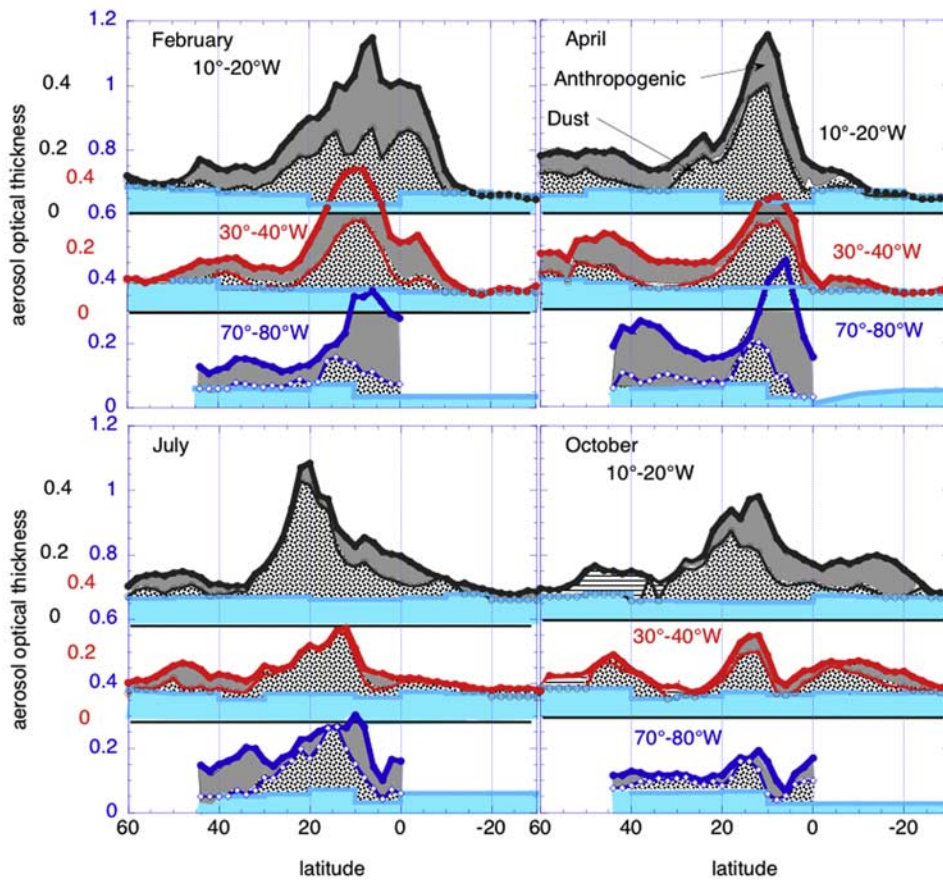
Figure 5. Latitudinal dependence of the monthly average aerosol total optical thickness (thick, topmost line in each panel), the anthropogenic portion (uniform gray area), dust portion (dotted area), and the maritime aerosol (marine-blue area) for 4 months (February, April, July, and October). The dashed area in the panel for October at high latitudes describes region of uncertainty where the MODIS data suggest a higher maritime aerosol optical thickness than computed with equation (2′). Note that the aerosol optical thickness is displayed as the sum of the maritime, dust, and anthropogenic contributions. The optical thickness and its components are computed from the MODIS aerosol measurements (equations (1)−(4)). Results are shown for longitudinal cross section at $10-20°W$, $30-40°W$, and $70-80°W$, averaged over the ocean only. The anthropogenic aerosol is maximum in February due to influx of biomass burning smoke from the Sahel and minimal in July. It is larger at $70-80°W$, owing to pollution and smoke from the Americas.

[17] The fraction of fine maritime aerosol, f_{ma}, of 0.3 is similar to analysis of AERONET data for the baseline maritime aerosol derived for the Pacific and Atlantic oceans [*Kaufman et al.*, 2001], and to in situ measurements [*Li et al.*, 1996]. The uncertainty represent the possible variation of f_{ma} as a function of the wind speed. The fraction of fine aerosol for dust (0.5) is also similar to AERONET analysis in Capo Verde (R. Kleidman et al., manuscript in preparation, 2004). We associate a smaller uncertainty to f_{du}, due to the little variation of dust size distribution as it crosses the Atlantic Ocean [*Maring et al.*, 2003].

[18] The error in the derived dust optical thickness in equation (4) is based on the validation of *Remer et al.* [2002] that the average error in τ is $\pm 0.01 \pm 0.05\tau$ or 10% for $\tau =$ 0.2. We estimate a similar error of 10% in $\tau(0.9\text{-}f)/0.4$ and, using Monte Carlo calculations get an error of $10-15\%$ in τ_{du} for $\tau_{du} > 0.1$. In some conditions, we may find MODIS measurements of optical thickness larger than the maritime contribution of equation (2′), but with fine mode fraction

much lower than what is measured by MODIS for dust. In such cases ($f < 0.4$) we assign the contribution to be uncertain of dust or maritime origin.

[19] Figure 5 shows the latitudinal dependence of the monthly average aerosol optical thickness and its division into maritime, dust and anthropogenic components. Three longitudinal cross sections across the Atlantic ocean are shown. Anthropogenic aerosol is maximum in February due to influx of biomass burning smoke from the Sahel, and is minimal in July. It is larger at $70°-80°W$ due to pollution and smoke from the Americas. Note that the higher dust concentration at $30°-60°N$ in April may be attributed to Asian dust transport over the United States that was particularly high in 2001 with dust optical thickness of 0.05 measured by lidar in mid April over the Washington Area ($40°N$, $75°W$) [*Welton et al.*, 2001].

[20] Figure 6 shows the monthly average dust optical thickness and total optical thickness, averaged over the dust belt ($0°-30°N$). The total optical thickness includes also
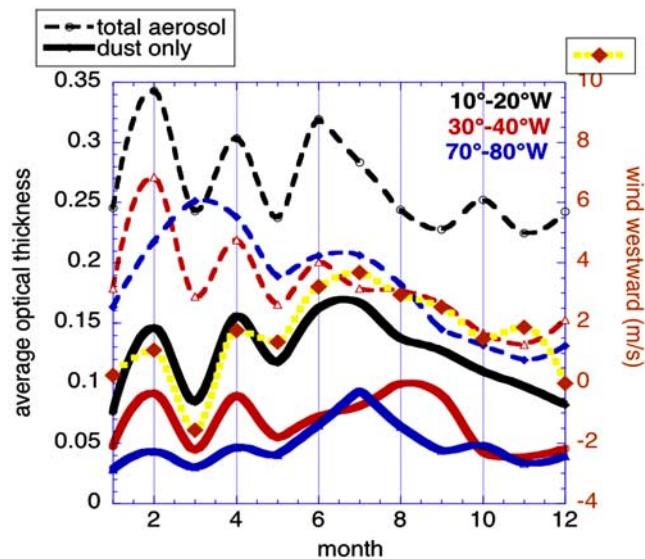
Figure 6. Monthly average dust optical thickness (solid lines) and total optical thickness (dashed lines) averaged on the dust belt (0°–30°N), for each month of 2001. Three longitudinal cross sections are shown: near the African coast (10°–20°W, black), near the South American coast (30°–40°W, red) and in the Caribbean (70°–80°W, blue). The monthly average dust optical thickness at 10°–20°W (solid black line) is compared with the monthly mean westward component of the wind velocity (yellow-orange line) derived from NCEP reanalysis data. The correlation is 80%. The winds were chosen from 700 mb for May–September [*Carlson and Prospero*, 1972] and 850 mb for October–April on the basis of analysis of *Chiapello et al.* [1995] and *Cakmur et al.* [2001]. Note that during June the data are available for only one week.

maritime and anthropogenic (mainly biomass burning) aerosol. Since strong winds are responsible for the dust mobilization and transport over the Atlantic Ocean, it can be anticipated that the dust component of the optical thickness will be influenced more by the winds than the total optical thickness. The kinetic energy used to release dust particles is proportional to the wind speed to the second power, while dust optical thickness, for a given emission rate is inversely proportional to the wind speed. Therefore we can expect, to a first order, a linear dependence of the dust concentration with the wind speed. In addition, for the cross section near the African coast, the correlation between the wind westward component and the average optical thickness increases from 25% for the total aerosol optical thickness to 80% for the dust component (Figure 6). Note that the process of smoke generation from man-made fires in Africa is not expected to produce smoke in proportionality to a power of the wind speed. The analysis shows that the maximum dust concentration near the coast of Africa occurs in the summer (June–August).

[21] The dust particles are transported westward across the Atlantic Ocean by the middle level easterly jet and sometimes north by the anticyclone over the Azores or Canaries Islands. The latitudinal variation of the dust belt is controlled by the movement of the west African midtropospheric jet [*Carlson and Prospero*, 1972; *Hastenrath*, 1986]

which occupies its northernmost position (20°N) in the summer. Figure 7 shows the latitudinal movement of the aerosol optical thickness during the three years of MODIS observations. It also shows the longitudinal transport and deposition of the dust (decrease in the optical thickness). Location of the maximum dust concentration varies from the equator in the winter (December–February) to 20°N in July, transporting the heaviest dust to the Caribbean islands and Florida [*Prospero and Carlson*, 1972; *Prospero*, 1999].

[22] The interannual variability of the dust optical thickness is also shown in Figures 8 and 9 Though for specific months (Figure 8) there is variability from year to year, the results show little difference between 2001, 2002 and 2003. The data in Figure 9 show that the seasonal average dust optical thickness for the summer season (May–October), averaged over the 3 years was 0.125 ± 0.015 and for the winter season (November–April) 0.085 ± 0.01. The variability represents 12% standard deviation among the three years.

4. Dust Transport and Deposition

[23] The dust column concentration, $M_{du}(g/m^2)$, is derived from the dust optical thickness, τ_{du}. In Appendix A we derive the ratio of the dust column mass to its optical thickness (A2):

$$M_{du}/\tau_{du} = 1.33\rho R_{eff}/Q = 2.7 \pm 0.4 \text{ g/m}^2, \qquad (6)$$

where τ_{du} is at 0.55 μm, ρ is the dust density, R_{eff} is the dust particle effective radius and Q is the light extinction efficiency. Using equations (4) and (5) the expression for the dust column concentration was derived in Appendix A (A4) as:

$$M_{du} = 2.7[\tau(0.9 - f)/0.4 - 1.5\tau_{ma}] \text{ g/m}^2, \qquad (7)$$

with a calculated uncertainty of ±30% for aerosol optical thickness in the 0.2–0.4 range.

[24] The NCEP reanalysis data set is used to calculate the dust transport. The winds are chosen for 700 mb (~3 km) for May–September as suggested by *Carlson and Prospero* [1972] and 850 mb (1.5 km) for October–April, based on analysis of *Chiapello et al.* [1995] and *Cakmur et al.* [2001]. Before applying the wind field data to the aerosol field, we performed several tests of the applicability of the wind field to the problem.

[25] In Figure 10 we plot the correlation between the westward component of the wind speed and the aerosol optical thickness in Capo Verde, downwind from the African dust. The correlation is high at altitudes of 2.6–5 km during the summer months of May through September. The correlation between the wind and dust optical thickness time series during the summer months is plotted in Figure 11. The correlation coefficient is drawing a vertical profile of the wind driven aerosol concentration: dust at the layer of 3–5 km and sea salt in the lowest 500 m. This correlation profile, serving as a "virtual lidar" concurs with the height selection for the wind field.

[26] In Figure 12 we look again on the correlation of dust optical thickness with the profile of the wind, but using this time the MODIS derived dust concentration, for several latitude bands. For latitudes with the highest dust concentra-
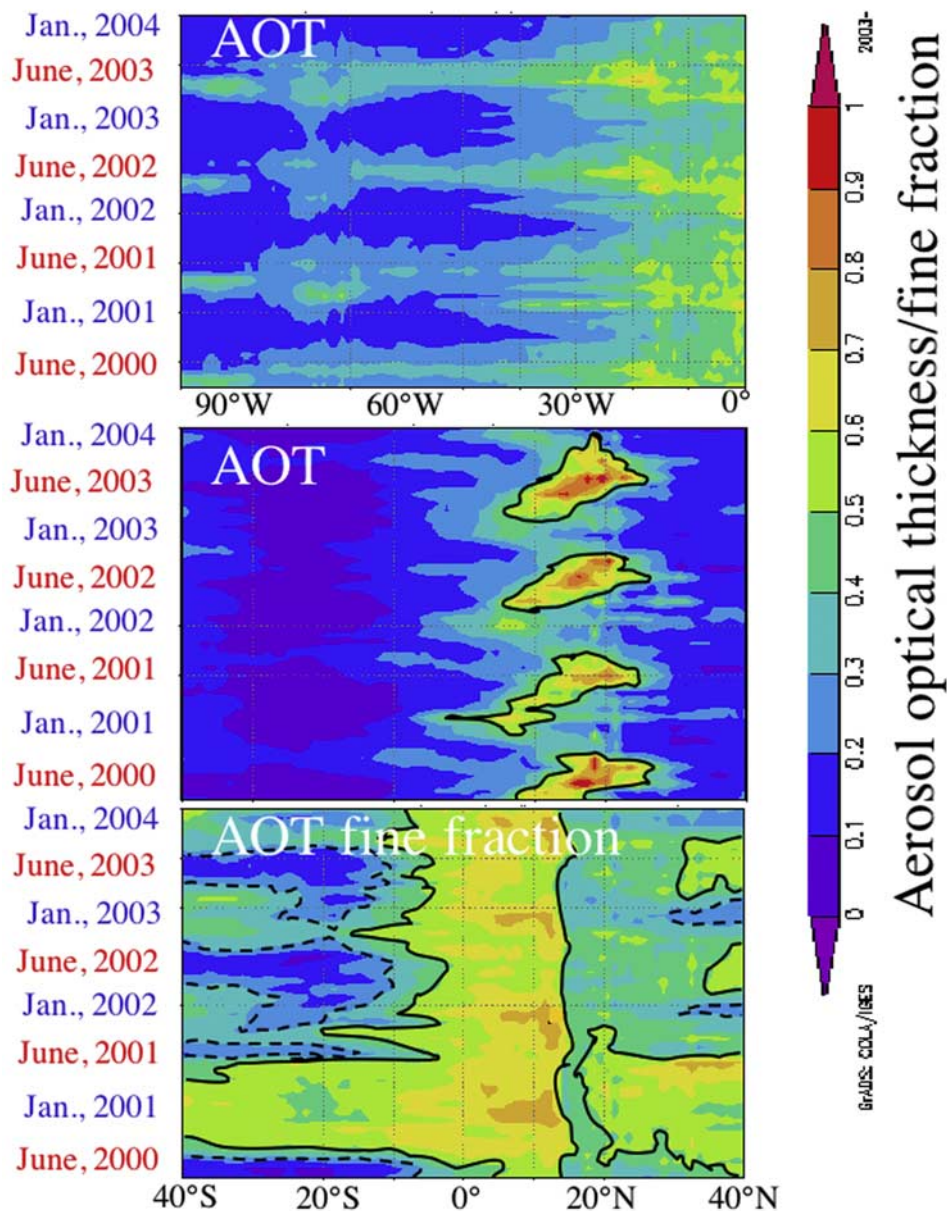
Figure 7. Aerosol optical thickness (see color bar on the right) as function of time (vertical axis), (top) longitude, and (center) latitude. The figures are averaged over 5°–20°N and or 15°–20°W, respectively. The top panel shows the annual dust transport westward from Africa to the Caribbean and deposition in the Atlantic Ocean, observed as a reduction in the optical thickness. The center panel shows the high dust emissions in May–September, with its maximum moving north from 7°N in February to 20°N in September. Contour line shows the value for optical thickness of 0.5. The bottom panel shows the fraction of the optical thickness attributed to the fine aerosol. Contour lines of the fine fraction of 0.5 (solid line) corresponding to dust and 0.3 (dashed lines), corresponding to maritime aerosol, are drawn. Note that the maritime air at 20°–40°S has fine fraction of 0.1–0.5 (average of 0.3 ± 0.1). Dust fine fraction is found at latitude of 20°N in the May–August as 0.5 ± 0.05. The images are constructed from monthly average data on the MODIS online Web site (http://lake.nascom.nasa.gov/movas/).

tion we also see the highest correlation with the wind speed. Note that in the winter there is no clear correlation with dust concentration in a given height for the measurements in Capo Verde, though in general the dust is expected to be closer to the surface as suggested by *Chiapello et al.* [1995].

[27] The actual wind speed can be tested against the rate of progression of the dust across the Atlantic Ocean, observed from two consequent MODIS observations, 3 hours apart one on Terra and second on the Aqua satellites. Example of the analysis is shown in Figure 13. The direction and speed of the dust transport is calculated by finding the shift of the Terra image relative to Aqua image. The direction of transport corresponds to altitude of 700 mb (3 km), however the NCEP wind speed is 15% slower than the rate
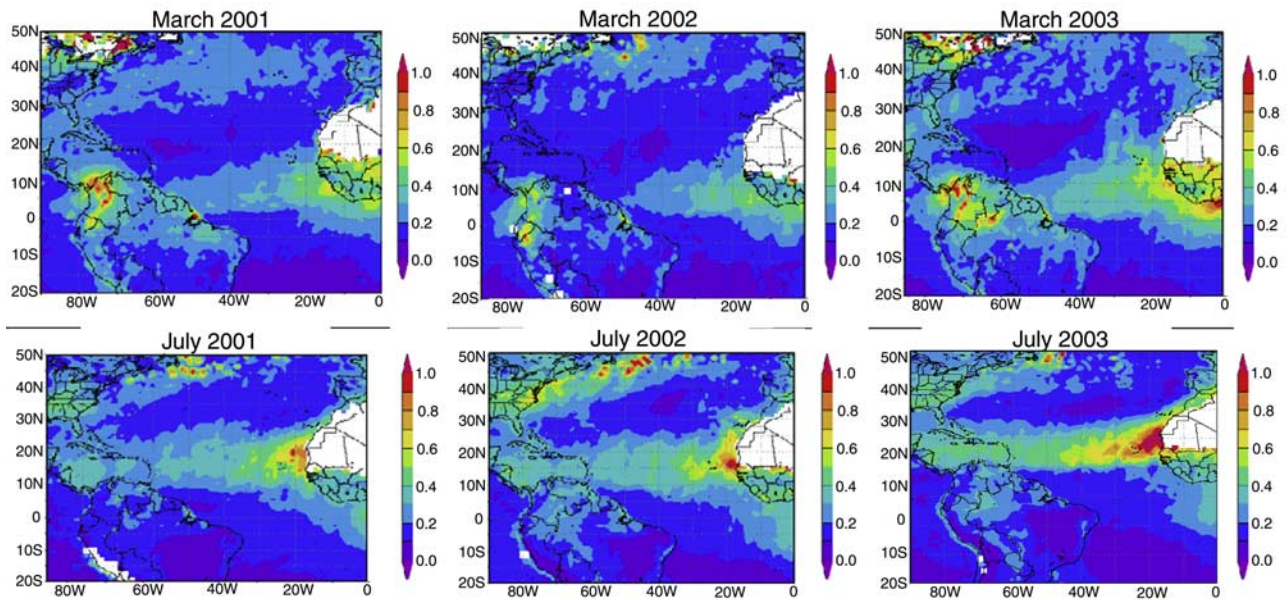
Figure 8. Spatial distribution of the aerosol optical thickness in the Atlantic dust belt. The maps are for 20°S–50°N and 0°–90°W for March 2001–2003 and July 2000–2002. There is little variability observed from one year to another. In March, dust and smoke transport is strongest in 2003, with larger northbound component and weakest in 2002. In July, with maximum transport, the results are similar for the 3 years. Note the dense pollution emitted from the east coast of the United States in 2003. Overall, the difference in average optical thickness between 2001 and 2002 was only 5%. The images were produced at the online website http://lake.nascom.nasa.gov/movas/.

of progression of the dust. Analysis of 4 such cases [*Koren and Kaufman*, 2004] shows that near the shore the NCEP wind speed underestimates the dust westward progression by 15% in the 5°–25°N dust belt. Further from the shore the winds did not match the dust progression analysis at all [*Koren and Kaufman*, 2004] at any height, raising large uncertainties in the dust transport calculations in the middle of the Atlantic Ocean.

[28] The flux, F, of dust transported from Africa at 15°W is calculated by applying the monthly average westward wind speed, W(m/s), to the monthly average dust concentration, M_{du}(g/m^2), and the longitudinal length, L (m), of the segment through which the flux is being computed (see discussion for the use of monthly mean values):

$$F(15°W) = M_{du}(15°W)W(15°W) \, L \, g/s \qquad (8)$$

[29] The units then can be transformed to Tg/month and applied also to the 35°W and 75°W transactions. The values of the seasonally averaged winds are shown in Table 1. The dust transport is summarized for the same two seasons in Table 2. The uncertainty in the fluxes reported in Table 2 result from uncertainty of ±30% in the dust concentration and uncertainty of ±15% in the wind speed near the continents, resulting in total uncertainty of ±35%. Deposition calculations are based on flux divergence. We assume that the errors in the flux are correlated and therefore the errors in deposition rates are still 35%.

[30] Overall 240 ± 80 Tg of dust are transported annually from Africa at 20°S–30°N. From that 20 ± 10 Tg return east to Africa and Europe at 30°N–50°N, 140 ± 40 Tg are deposited in the Atlantic Ocean, 50 ± 15 Tg are deposited in the Amazon Basin and 50 ± 25 Tg arrive to the Caribbean.

Table 2 and Figure 14 summarize these fluxes as a function of their geographic position. Note that out of the flux returning east, part can be attributed to Asian dust [*Welton et al.*, 2001].

[31] The net flux to the Amazon of 50 ± 15 Tg (35 in November–April and 15 in May–October; see Table 2), much larger than in the analysis of *Swap et al.* [1996] may explain the paradox that they found between the low estimate of dust deposition in the Amazon of 13 Tg and the order of magnitude larger estimate of the flux needed to sustain the forest. The present estimates of dust transport are more in line with the earlier estimates of *Prospero and Carlson* [1972].

[32] The results of dust deposition are compared with the models of *Prospero et al.* [1996], *Ginoux et al.* [2001, 2003], *Gao et al.* [2001] and *Fan et al.* [2004] in Table 3 and Figure 15. A good agreement is found between the dust deposition in the Atlantic Ocean as observed by MODIS and calculated in the Ginoux et al. model and the Fan et al. model for dust diameter ≤ 6 μm. The MODIS seasonal deposition is very similar to the seasonal deposition derived from the Ginoux et al. model.

5. Discussion

[33] The error analysis did not account several processes that can introduce additional uncertainty and are addressed here.

5.1. Monthly Averaging

[34] The first issue is the calculations of the dust fluxes across the longitudinal cross sections. The fluxes are calculated as the product of the monthly mean westward com-
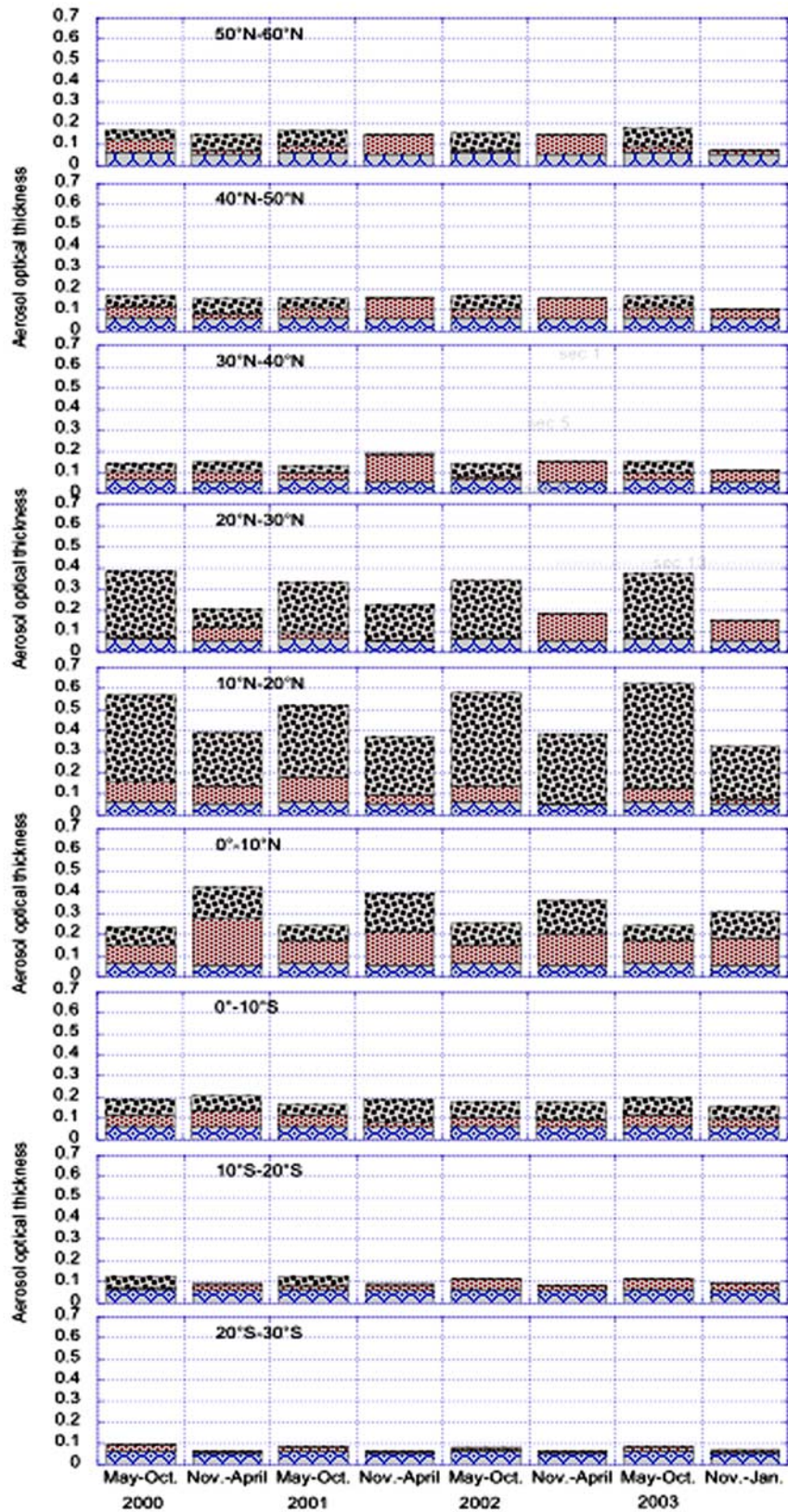
Figure 9. Four months average aerosol optical thickness from June 2000 to March 2003 classified as maritime (blue stripes, τ defined as 0.06), anthropogenic (red mash), and dust (brown mash) calculated from the monthly averaged optical thickness and the fraction of the optical thickness due to the fine aerosol. These data are taken from http://lake.nascom.nasa.gov/movas/. The separation to maritime anthropogenic and dust components was performed using equation (4).
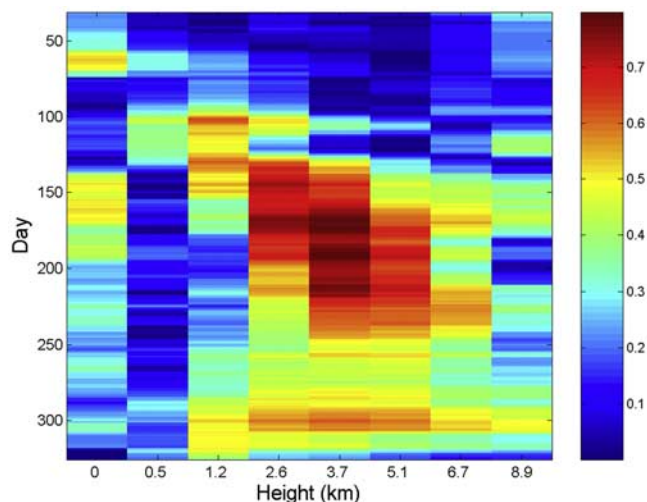
Figure 10. Correlation between the westward component of the wind speed taken from the NCEP reanalysis and the aerosol optical thickness measured by AERONET in Capo Verde. The correlation (color bar on the right) is calculated for 2 months running sequences of wind and aerosol data only with aerosol optical thicknesses for Ångström exponent <0.3. Note the high correlations between the aerosol optical thickness and the wind speed at altitudes of 2.6–5 km during May–September. One hundred and sixty measurements were used in the analysis.

ponent of the wind and the dust mass column concentration. This approach can be valid if the correlation between dust concentration and wind speed does not affect the monthly flux. Therefore we need to check if the flux given by equation (8), F_M, for the product of the monthly averages

Figure 12. Scatterplots of the monthly average dust column concentration as a function of the monthly average westward wind speed for four latitude ranges as indicated and a longitudinal cross section at $10°–20°W$. Each point represents a monthly average for winds at 750 mb. The correlation between the wind speed and the dust concentration varies between 80% for the region with the highest dust concentration and 0% for linear correlation at $30°–40°N$.

$\langle M_{du} \rangle$ for dust concentration and $\langle W \rangle$ for average westward component of the wind, is equal to the accurate estimate using the daily data of MODIS dust concentration and winds. Therefore, defining

$$F_M = \langle M_{du} \rangle \langle W \rangle L \quad \text{and} \quad \langle F_D \rangle = \langle M_{du} W \rangle L,$$
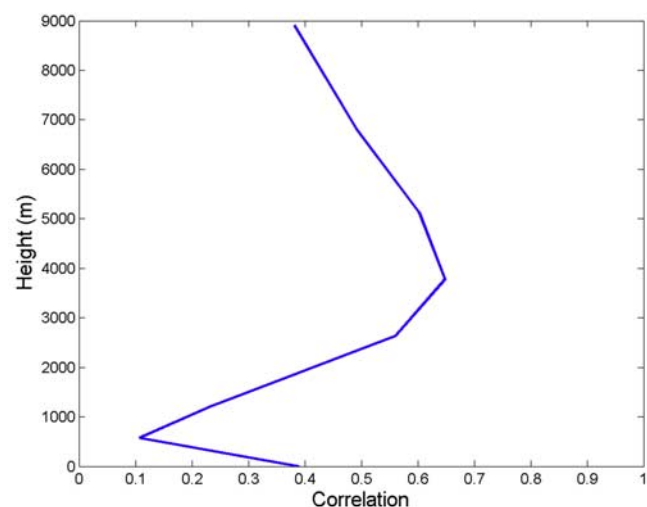

Figure 11. Correlation between the wind and dust optical thickness time series measured in Capo Verde during the summer months. One hundred and fifteen measurements were used in the analysis. The correlation coefficient is drawing a profile of the wind driven aerosol. Dust was at the layer of 3–5 km, and sea salt was in the lowest 500 m. This correlation profile serves as a virtual lidar that draws the concentration of the wind driven aerosol.
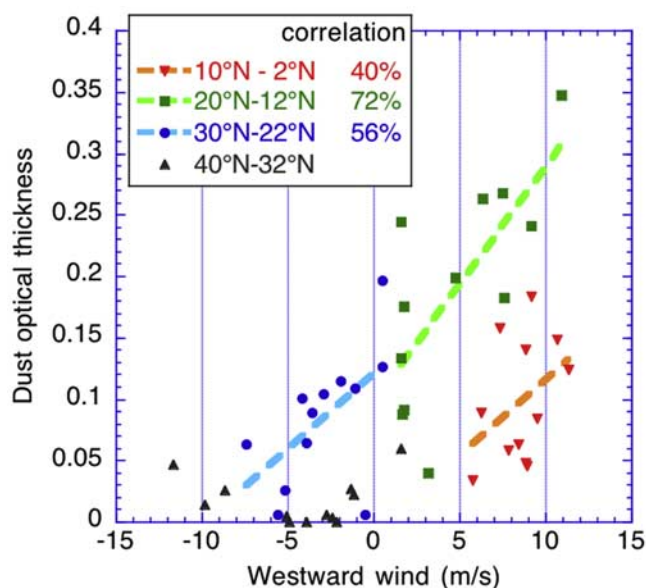

Figure 13. Dust classified in the MODIS images from Terra and Aqua images of Figure 2 for 1 May 2003 (color images on the left). The westward shift of the dust plume between the two observations taken 3 hours apart is 120 km, corresponding to wind speed of 11 m/s. The NCEP winds for that day were 7.5 and 10 m/s for 850 (1.5 km) and 700 mb (3 km). The MODIS data show direct westward progression. This wind direction corresponds to NCEP winds at 750 mb (interpolated between 850 and 700) with wind speed of 9.2 m/s. Right panel shows NCEP wind field at 700 mb.

Table 1. Average Westward Component of the Wind Velocity (m/s) at 850 mb for October–April and 700 mb for May–September From the NCEP Reanalysis Data for Two Parts of the Year and for Three Longitudinal Cross Sections Across the Atlantic Ocean

Period	10°–20°S	0°–8°S	0°–10°N	10°–20°N	20°–30°N	30°–40°N	40°–50°N
			10°–20°W: West African Coast				
Oct.–Apr.	5.4	5.1	3.9	4.2	1.2	−2.5	−5.3
May–Sept.	3.5	4.1	6.9	9.9	−0.8	−4.1	−6.9
			30°–40°W: Eastern South American Coast				
Oct.–Apr.	5.4	7.9	8.2	6.5	1.6	−4.7	−7.6
May–Sept.	2.9	5.2	6.1	7.8	1.9	−4.3	−9.5
			70°–80°W: Caribbean				
Oct.–Apr.		2.0	7.3	1.1	−6.4		
May–Sept.		6.0	7.0	0.7	−4.6		

we need to check if

$$F_M = \langle F_D \rangle. \qquad (9)$$

In Figure 16 we compare the monthly average wind speed $\langle W \rangle$ with wind speed weighted by the dust concentration (for simplicity the aerosol optical thickness was used as the weighting factor):

$$W_w = \langle M_{du} W \rangle / \langle M_{du} \rangle. \qquad (10)$$

Thus if $W_w \approx \langle W \rangle$ then $F_M \approx \langle F_D \rangle$. The result, shown for four pressure levels, show that $W_w \approx \langle W \rangle$ on average within 5%.

5.2. Maritime Aerosol

[35] The second issue is the use of specific wind-dependent maritime aerosol optical thickness. There were several publications that indicated the dependence of maritime aerosol extinction coefficient on the wind speed. We use *Smirnov et al.* [2003] analysis of AERONET data to relate the column optical thickness to the wind speed in Midway Island (equation (2′)). *Smirnov et al.* [2003] also reviewed other studies and deduced from them values of the slope of optical thickness with speed of 0.002 to 0.008.

5.3. Diurnal Cycle

[36] A dust persistent diurnal cycle could generate an error in the monthly and annual estimates presented here. It was already reported [*Kaufman et al.*, 2000] that on global basis the Terra measurements at ∼1030 LT or the Aqua measurements at 1330 LT do represent the daily average for any range of aerosol optical thicknesses or particle size

(described there by the Ångström exponent). However, in locations close to aerosol sources the daily cycle may be significant. Capo Verde is the closest maritime measurements to the African sources and was shown by *Smirnov et al.* [2002] to have a diurnal cycle <5% of the optical thickness. Figure 17 tests this relationship. The AERONET data here are monthly averaged using measurements throughout the day while the MODIS data are centered on 1030 LT. Though some differences are due to spatial inhomogeneity or differences of AERONET to MODIS, on annual average MODIS is higher than AERONET by 4% in 2001 and lower than AERONET by 5% in 2002.

6. Conclusions

[37] The interest in desert dust research and its effects on climate, ocean and land productivity, air pollution and atmospheric chemistry increased exponentially in the last 30 years, bringing abundant information on the dust optical/physical, and chemical properties. Already in the early works of Prospero and Carlson, the importance of satellite data in mapping the extent of the dust spread and transport was recognized and they were coupled with ground based and aircraft samplings to estimate the rate of dust emission transport and deposition.

[38] The recent introduction of data from the MODIS instrument flown on Terra and Aqua satellites introduces a new instrument with important capability for quantitative dust measurements. MODIS accuracy and spectral sampling across the solar spectrum, together with several years of dust remote sensing from the ground by AERONET, allows accurate measurements of the aerosol optical thickness and distinction between anthropogenic aerosol, dominated by

Table 2. Dust Flux Through the Longitudinal Cross Sections for Each Segment of 10° Latitude in Tg of Mass of Dust for the Indicated Period

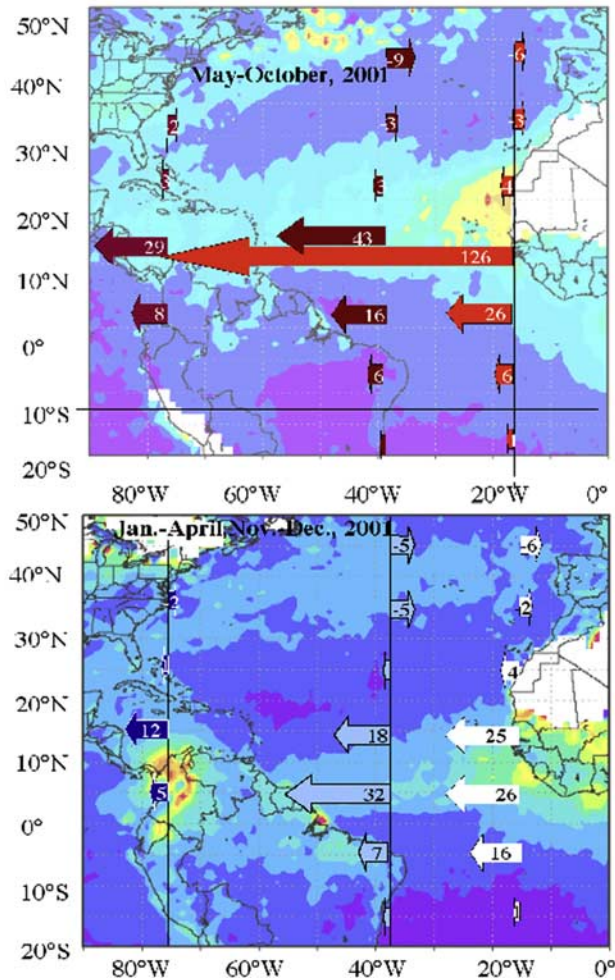| Period	20°–10°S	10°S–0°	0°–10°N	10°–20°N	20°–30°N	30°–40°N	40°–50°N	Total
		10°W–20°W: West African Coast Annual Flux, 218 Tg/year						
Nov.–Apr.	1	16	26	25	4	−2	−6	64
May–Oct.	1	6	26	126	4	−3	−6	154
	30°W–40°W Annual Flux: 63 Tg/year to the Amazon (0°–10°N) and 43 Tg/year to Caribbean–North America (10°N–50°N)							
Nov.–Apr.	1	7	32	18	1	−5	−5	49
May–Oct.	1	6	16	43	3	−3	−9	57
			70°W–80°W: Caribbean Annual Flux 54 Tg/year					
Nov.–Apr.			5	12	1	−2		16
May–Oct.			8	29	3	−2		38

Figure 14. Graphical representation of dust transport (Tg) across the Atlantic Ocean for (top) May–September and for (bottom) October–April on the background of MODIS image from July and March 2001, respectively, for three longitudinal cross sections at 15°W, 35°W, and 75°W. Note that near the continents the wind field and the corresponding dust transport are more reliable.

fine submicron particles and dust or maritime aerosol with large fraction of coarse supermicron particles.

[39] We reported here calculations of the dust monthly and annual transport from Africa and deposition in the Atlantic Ocean. The analysis reveals on a regional scale (Figure 6) the large fraction of biomass burning smoke

imbedded in the dust in the winter months (45% smoke & 55% dust in December–March) due to savanna fires in the Sahel, with purer dust (14% smoke, 86% dust) transported from Africa in the summer months (June–September).

[40] The peculiar monthly oscillation of the dust transport with maxima and minima regularly oscillating between January and June was found to be easily explainable with similar oscillations of the monthly average wind westward component. The correlation of the wind with the dust column concentration is 80% (Figure 12). The wind height selection at 700 mb (3–5 km) in May–October and 850 mb (0–1 km) in November based on the literature was reaffirmed using a similar correlation between winds and dust from AERONET data in Capo Verde (Figure 10).

[41] The results (Figure 7) confirm the migration of the dust center of gravity from close to the equator in the January to 20°N in September and back to the equator in December. In December–March dust is transported across the Atlantic Ocean to the Amazon Basin both below and above the equator. The 50 Tg of dust deposited in the Amazon, much larger than in the analysis of *Swap et al.* [1996] may explain the paradox described by *Swap et al.* [1996] between the need of nutrition by the Amazon forest and the source of the nutrition – the Saharan dust.

[42] The annual dust deposition in 2001 of 144 Tg derived from the MODIS analysis is almost identical with the analysis of GOCART for the same year of 143 Tg, and 140 Tg of *Fan et al.* [2004] model for particles <6 μm. *Prospero et al.* [1996] suggested for the general climatology 170 Tg. Maximum deposition occurs in the summer, less is deposited in the fall and minimum deposition occurs in the spring and winter. This annual cycle agrees with the *Ginoux et al.* [2001] GOCART model and to a large degree also with the *Gao et al.* [2001] and *Fan et al.* [2004] models. The interannual variation between 2000 and 2003 was found to be only 12% in the MODIS data (Figure 9).

Appendix A: Conversion From Dust Optical Thickness to Mass Column Concentration

[43] The dust mass column concentration is calculated from the optical thickness, using the following relationships between the dust mass and optical thickness to the dust size distributions:

$$M_{du} = (\rho 4\pi/3) \int r^3 n(r)dr; \tau_{du} = \pi \int Q(r)r^2 n(r)dr, \quad (A1)$$

where n(r) is the particle size distribution, ρ is specific weight and Q is the light extinction efficiency. For the large

Table 3. Comparison of Dust Deposition During Four Seasons for 0°–40°N Between MODIS Data, the Model of *Fan et al.* [2004], the GOCART Model of *Ginoux et al.* [2001, 2003], and the Results of *Gao et al.* [2001] and *Prospero et al.* [1996][a]

Season	Fan et al. [2004] 0.2–6 μm	Fan et al. [2004] 0.2–12 μm	Ginoux et al. [2001], Tg	MODIS, Tg	Gao et al. [2001] Iron, Tg	Gao et al. [2001] Dust, Tg	Prospero et al. [1996]
Spring	29	56	29	10	1.4	41	
Summer	53	111	48	51	2.5	72	
Fall	28	55	41	60	2.3	66	
Winter	30	62	24	23	0.9	25	
Total	140	284	143	144	7	204	170

[a]*Gao et al.*'s [2001] dust deposition was reconstructed from their iron deposition calculations for 3.5% fraction of iron in the dust. Except for *Prospero et al.* [1996], the results are given for 2001.
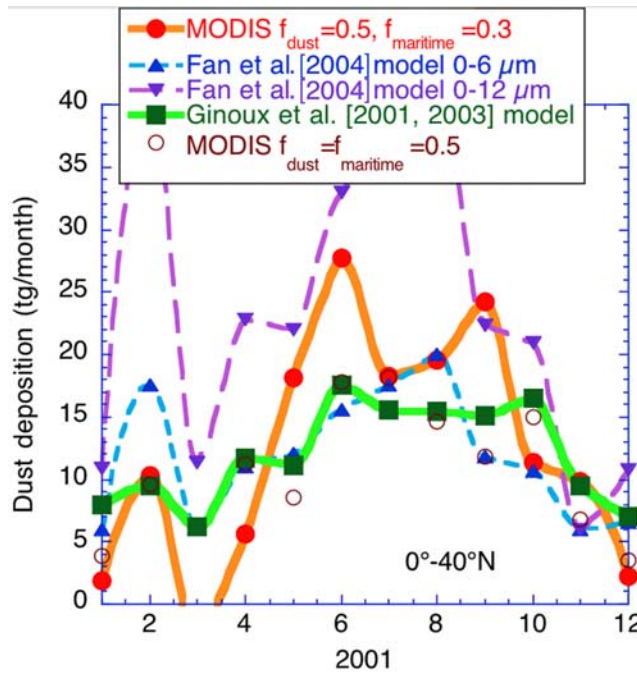
Figure 15. Dust deposition rates (Tg/month) derived from MODIS measurements and calculated by the chemical transport models of *Ginoux et al.* [2001, 2003] and *Fan et al.* [2004] for the region (0°−40°N). For MODIS, two sets of assumption are used as indicated in the legend.

dust effective radius of 1.7 to 2.0 μm (size parameter X = $2\pi r/\lambda \sim 20$) obtained from inversion of AERONET data [*Tanré et al.*, 2001] and measured in situ [*Maring et al.*, 2003, hereinafter referred to as M03], respectively, Q ~ 2.2. Calculations by the GOCART model [*Ginoux et al.*, 2001,
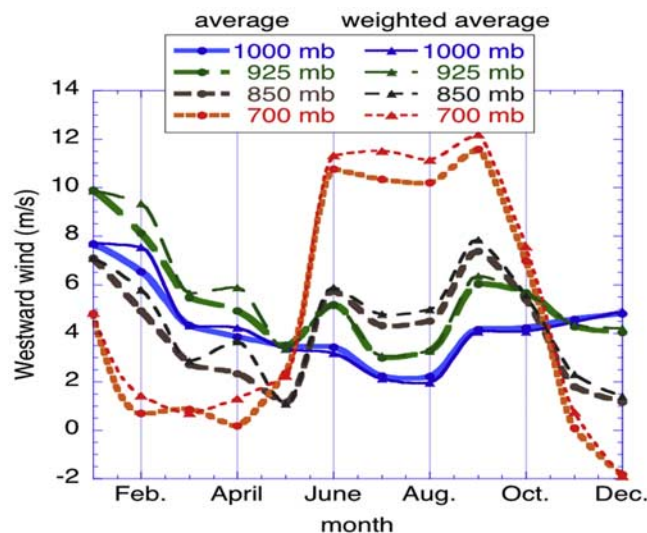

Figure 16. Annual cycle of the monthly average westward component of the wind for four pressure levels. The average wind speed was calculated by two methods: simple monthly average around the satellite pass time of 0930 GMT for the longitude of 15°W and weighted average, with the weight being the aerosol optical thickness measured by MODIS.
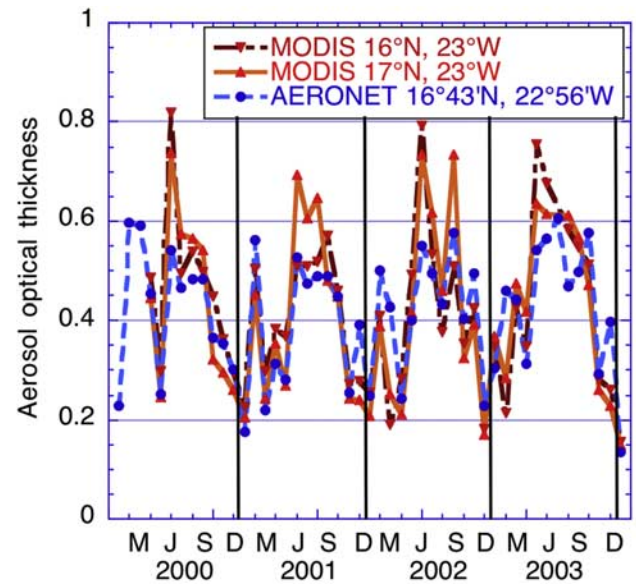

Figure 17. Monthly averages of the aerosol optical thickness measured by AERONET in Capo Verde and derived from MODIS around the location of the Sun photometer over the ocean. For the 3 full years of operation the MODIS optical thickness was 0.40−0.42, and AERONET was 0.39−0.43. The MODIS data are from Terra at ~1030 LT, and the AERONET data are averaged on the daily hours. The AERONET level 1.0 data are used with only partial cloud screening due to possible screening of heavy dust with the accompanied clouds. Both data sets show similar seasonal cycle of the aerosol with maximum in the June−September time frame.

2004] and by the model of *Fan et al.* [2004] show similar volume mean radius of 1.3 to 1.8 μm. Assuming Q is independent of radius for dust, the ratio of the dust mass to the dust optical thickness can be expressed by:

$$M_{du}/\tau_{du} = 1.33\rho R_{eff}/Q, \text{ where } R_{eff} = \int r^3 n(r)dr / \int r^2 n(r)dr. \quad (A2)$$

The specific weight is reported as $\rho = 2.0$ g/cm^3 by MO3 and $\rho = 2.6$ g/cm^3 by *Haywood et al.* [2003]. *Haywood et al.* [2003] measured average extinction efficiency of 0.37 cm^3/g, corresponding to $M/\tau_{du} = 2.7$ g/m^2. Note that the set of parameters taken from MO3: of $\rho = 2.0$ g/cm^3, $R_{eff} = 2$ μm $Q = 2$ gives the same value of $M/\tau_{du} = 2.7$ g/m^2. Also *Haywood et al.* [2003] $\rho = 2.6$ g/cm^3, combined with AERONET $R_{eff} = 1.7$ μm and $Q = 2.2$ also gives $M/\tau_{du} = 2.7$ g/m^2. Therefore $M/\tau_{du} = 2.7$ g/m^2 is the "popularly selected" ratio used here. Monte Carlo calculations for uncertainty of 10% in τ and R_{eff} and 5% in Q suggest uncertainty in the ratio M/τ of ±0.4.

[44] Several authors reported measurement of the extinction or scattering efficiency derived from the ratio of the extinction or scattering coefficient to the dust mass. *Moulin et al.* [1997b] reviewed dust models giving 0.6−0.8 m^2/g, corresponding to M/τ of 1.2−1.7 g/m^2. *Chin et al.* [2002] used also 0.8 m^2/g in their dust calculations. MO3 derived 0.5 m^2/gr near Africa and inferred 0.6 m^2/g in Barbados

from measurements of *Li et al.* [1996], corresponding to M/τ of 2.0 and 1.7 g/m^2, *Dulac et al.* [1992] noted the large uncertainty in the value and used 1.3 g/m^2 somewhat lower than the values used here. On the other hand, *Carlson* [1979] used a higher value of $M/\tau = 3.6$ g/m^2. The small reduction in dust size from the African coast to the Caribbean suggest reduction of M/τ across the Atlantic. Since the magnitude of the reduction is 15% or smaller, and smaller than uncertainty in M/τ, we did not include it in the calculations.

[45] To derive the equation for the dust column mass concentration we first substitute the values of the fine fraction from equation (5) into equation (4) to get a compact solution for the dust optical thickness:

$$\tau_{du} = [\tau(0.9 - f)/0.4 - 1.5\tau_{ma}], \qquad (A3)$$

and applying the mass/optical thickness ratio: $M/\tau_{du} = 2.7 \pm 0.4$ g/m^2 we get

$$M_{du} = (2.7 \pm 0.4)[\tau(0.9 - f)/0.4 - 1.5\tau_{ma}] \qquad g/m^2. \quad (A4)$$

[46] The uncertainties in the mass calculations, ΔM_{du}, are due to errors in the M/τ ratio of ± 0.4 g/m^2, the regionally average total optical thickness $-\Delta\tau/\tau = \pm 10$, the fraction $[(0.9-f)/0.4]$ of $\pm 10\%$, and an error in the marine optical thickness - $\Delta\tau_{ma} = \pm 0.005$. Monte Carlo calculations give total error of $\pm 30\%$ for aerosol optical thickness of 0.2 to 0.4. These two optical thicknesses correspond to the regional average dust optical thickness and to the center of the dust respectively.

References

Alpert, P., et al. (1998), Quantification of dust-forced heating of the lower troposphere, *Nature*, 395, 367–370.

Alpert, P., et al. (2002), A dust prediction system with TOMS initialization, *Mon. Weather Rev.*, 130(9), 2335–2345.

Barnes, W. L., T. S. Pagano, and V. V. Salomonson (1998), Pre-launch characteristics of MODIS on EOS-AM1, *IEEE Trans. Geosci. Remote Sens.*, 36, 1088–1100.

Cakmur, R. V., R. L. Miller, and I. Tegen (2001), A comparison of seasonal and interannual variability of soils dust aerosols over the Atlantic Ocean as inferred by the TOMS AI and AVHRR AOT retrievals, *J. Geophys. Res.*, 106(D16), 18,287–18,303.

Carlson, T. N. (1979), Atmospheric turbidity in Saharan dust outbreaks as determined by analysis of satellite brightness data, *Mon. Weather Rev.*, 107, 322–335.

Carlson, T. N., and J. M. Prospero (1972), The large scale movement of Saharan air outbreaks over the northern equatorial Atlantic, *J. Appl. Meteorol.*, 11, 283–297.

Chiapello, I., and C. Moulin (2002), TOMS and METEOSAT satellite records of the variability of Saharan dust transport over the Atlantic during the last two decades (1979–1997), *Geophys. Res. Lett.*, 29(8), 1176, doi:10.1029/2001GL013767.

Chiapello, I., et al. (1995), An additional low layer transport of Sahelian and Saharan dust over the northeastern tropical Atlantic, *Geophys. Res. Lett.*, 22, 3191–3194.

Chiapello, I., J. M. Prospero, J. R. Herman, and N. C. Hsu (1999), Detection of mineral dust over the North Atlantic Ocean and Africa with the Nimbus 7 TOMS, *J. Geophys. Res.*, 104, 9277–9292.

Chin, M., et al. (2002), Tropospheric aerosol optical thickness from the GOCART model and comparisons with satellite and Sun photometer measurements, *J. Atmos. Sci.*, 59, 461–483.

Dentener, F. J., G. R. Carmichael, Y. Zhang, J. Lelieveld, and P. J. Crutzen (1996), Role of mineral aerosol as a reactive surface in the global troposphere, *J. Geophys. Res.*, 101, 22,869–22,889.

Dulac, F., et al. (1992), Assessment of the African airborne dust mass over the western Mediterranean Sea using Meteosat data, *J. Geophys. Res.*, 97, 2489–2506.

Erickson, D. J., III, J. L. Hernandez, P. Ginoux, W. W. Gregg, C. McClain, and J. Christian (2003), Atmospheric iron delivery and surface ocean biological activity in the Southern Ocean and Patagonian region, *Geophys. Res. Lett.*, 30(12), 1609, doi:10.1029/2003GL017241.

Fan, S., L. W. Horowitz, H. Levy II, and W. J. Moxim (2004), Impact of air pollution on wet deposition of mineral dust aerosols, *Geophys. Res. Lett.*, 31, L02104, doi:10.1029/2003GL018501.

Gao, Y., et al. (2001), Seasonal distributions of aeolian iron fluxes to the global ocean, *Geophys. Res. Lett.*, 28, 29–32.

Ginoux, P., and O. Torres (2003), Empirical TOMS index for dust aerosol: Applications to model validation and source characterization, *J. Geophys. Res.*, 108(D17), 4534, doi:10.1029/2003JD003470.

Ginoux, P., et al. (2001), Sources and distributions of dust aerosols simulated with the GOCART model, *J. Geophys. Res.*, 106, 20,255–20,274.

Ginoux, P., J. M. Prospero, O. Torres, and M. Chin (2003), Long-term simulation of global dust distribution with the GOCART model: Correlation with the North Atlantic Oscillation, *Environ. Model. Software*, doi:10.1016/S1364-8152(03)00114-2.

Hastenrath, S. (1986), On climate prediction in the tropics, *Bull. Am. Meteorol. Soc.*, 67(6), 696–702.

Haywood, J., P. Francis, S. Osborne, M. Glew, N. Loeb, E. Highwood, D. Tanré, G. Myhre, P. Formenti, and E. Hirst (2003), Radiative properties and direct radiative effect of Saharan dust measured by the C-130 aircraft during SHADE: 1. Solar spectrum, *J. Geophys. Res.*, 108(D18), 8577, doi:10.1029/2002JD002687.

Herman, J. R., et al. (1997), Global distribution of UV-absorbing aerosol from Nimbus-7/TOMS data, *J. Geophys. Res.*, 102, 16,911–16,922.

Holben, B. N., J. Kandell, and Y. J. Kaufman (1990), Calibration of NOAA-11 AVHRR visible and near-IR bands, *Int. J. Remote Sens.*, 11, 1511–1519.

Hsu, N. C., et al. (1996), Detection of biomass burning smoke from TOMS measurements, *Geophys. Res. Lett.*, 23, 745–748.

Husar, R. B., J. M. Prospero, and L. L. Stowe (1997), Characterization of tropospheric aerosols over the oceans with the NOAA advanced very high resolution radiometer optical thickness operational product, *J. Geophys. Res.*, 102, 16,889–16,909.

Ignatov, A., and L. Stowe (2002), Aerosol retrievals from individual AVHRR channels. part I: Retrieval algorithm and transition from Dave to 6S radiative transfer model, *J. Atmos. Sci.*, 59, 313–334.

Jankowiak, I., and D. Tanré (1992), Satellite climatology of Saharan dust outbreaks, *J. Clim.*, 5, 646–656.

Karyampudi, M. V., et al. (1999), Validation of the Saharan dust plume conceptual model using Lidar, METEOSAT, and ECMWF data, *Bull. Am. Meteorol. Soc.*, 80, 1045–1076.

Kaufman, Y. J., et al. (1997), Remote sensing of tropospheric aerosol from EOS-MODIS over the land using dark targets and dynamic aerosol models, *J. Geophys. Res.*, 102, 17,051–17,067.

Kaufman, Y. J., et al. (2000), Will aerosol measurements from Terra and Aqua polar orbiting satellites represent the daily aerosol abundance and properties?, *Geophys. Res. Lett.*, 27, 3861–3864.

Kaufman, Y. J., A. Smirnov, B. N. Holben, and O. Dubovik (2001), Baseline maritime aerosol: Methodology to derive the optical thickness and scattering properties, *Geophys. Res. Lett.*, 28, 3251–3254.

Kaufman, Y. J., D. Tanré, and O. Boucher (2002), A satellite view of aerosols in the climate system, *Nature*, 419, 215–223.

King, M. D., Y. J. Kaufman, D. Tanré, and T. Nakajima (1999), Remote sensing of tropospheric aerosols from space: Past, present and future, *Bull. Am. Meteorol. Soc.*, 80, 2229–2259.

King, M. D., et al. (2003), Cloud and aerosol properties, precipitable water, and profiles of temperature and humidity from MODIS, *IEEE Trans. Geosci. Remote Sens.*, 41, 442–458.

Koren, I., and Y. J. Kaufman (2004), Direct wind measurements of Saharan dust events from Terra and Aqua satellites, *Geophys. Res. Lett.*, 31, L06122, doi:10.1029/2003GL019338.

Levin, Z., E. Ganor, and V. Gladstein (1996), The effects of desert particles coated with sulfate on rain formation in the eastern Mediterranean, *J. Appl. Meteorol.*, 35, 1511–1523.

Li, X., H. Maring, D. Savoie, K. Voss, and J. M. Prospero (1996), Dominance of mineral dust in aerosol light scattering in the North Atlantic trade winds, *Nature*, 380, 416–419.

Maring, H., D. L. Savoie, M. A. Izaguirre, L. Custals, and J. S. Reid (2003), Mineral dust aerosol size distribution change during atmospheric transport, *J. Geophys. Res.*, 108(D19), 8592, doi:10.1029/2002JD002536.

Martin, J. H., R. M. Gordon, and S. E. Fitzwater (1991), The case for iron, *Limnol. Oceanogr.*, 36, 1793–1802.

Martin, R. V., D. J. Jacob, R. M. Yantosca, M. Chin, and P. Ginoux (2003), Global and regional decreases in tropospheric oxidants from photochemical effects of aerosols, *J. Geophys. Res.*, *108*(D3), 4097, doi:10.1029/2002JD002622.

Martins, J. V., D. Tanré, L. Remer, Y. Kaufman, S. Mattoo, and R. Levy (2002), MODIS Cloud screening for remote sensing of aerosols over oceans using spatial variability, *Geophys. Res. Lett.*, *29*(12), 8009, doi:10.1029/2001GL013252.

Moulin, C., C. E. Lambert, F. Dulac, and U. Dayan (1997a), Control of atmospheric export of dust from North Africa by the North Atlantic Oscillation, *Nature*, *387*, 691–694.

Moulin, C., et al. (1997b), Long term daily monitoring of Saharan dust load over ocean using Meteosat ISCCP-B2 data, 12, accuracy of the data and validation using Sun photometer measurements, *J. Geophys. Res.*, *102*, 16,959–19,969.

Pinker, R. T., et al. (2001), A dust outbreak episode in sub-Sahel West Africa, *J. Geophys. Res.*, *106*, 22,923–22,930.

Prospero, J. M. (1999), Long term measurements of the transport of African mineral dust to the southern United States: Implications for regional air quality, *J. Geophys. Res.*, *104*, 15,917–15,927.

Prospero, J. M., and T. N. Carlson (1972), Vertical and areal distribution of Saharan dust over the western equatorial North Atlantic ocean, *J. Geophys. Res.*, *77*, 5255–5265.

Prospero, J. M., and P. J. Lamb (2003), African droughts and dust transport to the Caribbean: Climate change implications, *Science*, *302*, 1024–1027.

Prospero, J. M., and R. T. Nees (1977), Dust concentration in the atmosphere of the equatorial North Atlantic Possible relationship to Sahelian drought, *Science*, *196*, 1196–1198.

Prospero, J. M., R. A. Glaccum, and R. T. Nees (1981), Atmospheric transport of soil dust from Africa to South America, *Nature*, *289*, 570–572.

Prospero, J. M., et al. (1996), Atmospheric deposition of nutrients to the North Atlantic basin, *Biogeochemistry*, *35*, 27–73.

Prospero, J. M., P. Ginoux, O. Torres, S. E. Nicholson, and T. E. Gill (2002), Environmental characterization of global sources of atmospheric soil dust identified with the NIMBUS 7 Total Ozone Mapping Spectrometer (TOMS) absorbing aerosol product, *Rev. Geophys.*, *40*(1), 1002, doi:10.1029/2000RG000095.

Ramanathan, V., et al. (2001), The Indian Ocean Experiment: An integrated analysis of the climate forcing and effects of the great Indo-Asian haze, *J. Geophys. Res.*, *106*, 28,371–28,398.

Remer, L. A., et al. (2002), Validation of MODIS aerosol retrieval over ocean, *Geophys. Res. Lett.*, *29*(12), 8008, doi:10.1029/2001GL013204.

Rosenfeld, D., Y. Rudich, and R. Lahav (2001), Desert dust suppressing precipitation—A possible desertification feedback loop, *Proc. Natl. Acad. Sci.*, *98*, 5975–5980.

Smirnov, A., B. N. Holben, T. F. Eck, I. Slutsker, B. Chatenet, and R. T. Pinker (2002), Diurnal variability of aerosol optical depth observed at AERONET (Aerosol Robotic Network) sites, *Geophys. Res. Lett.*, *29*(23), 2115, doi:10.1029/2002GL016305.

Smirnov, A., B. N. Holben, T. F. Eck, O. Dubovik, and I. Slutsker (2003), Effect of wind speed on columnar aerosol optical properties at Midway Island, *J. Geophys. Res.*, *108*(D24), 4802, doi:10.1029/2003JD003879.

Stanhil, G. (2001), The growth of climate change science: A scientometric study, *Clim. Change*, *48*, 515–524.

Swap, R., et al. (1992), Saharan dust in the Amazon basin, *Tellus, Ser. B*, *44*, 133–149.

Swap, R., S. Ulanski, M. Cobbett, and M. Garstang (1996), Temporal and spatial characteristics of Saharan dust outbreaks, *J. Geophys. Res.*, *101*, 4205–4220.

Tanré, D., M. Herman, and Y. J. Kaufman (1996), Information on aerosol size distribution contained in solar reflected radiances, *J. Geophys. Res.*, *101*, 19,043–19,060.

Tanré, D., Y. J. Kaufman, M. Herman, and S. Mattoo (1997), Remote sensing of aerosol over oceans from EOS-MODIS, *J. Geophys. Res.*, *102*, 16,971–16,988.

Tanré, D., et al. (1999), Retrieval of aerosol optical thickness and size distribution over ocean from the MODIS airborne simulator during TARFOX, *J. Geophys. Res.*, *104*, 2261–2278.

Tanré, D., et al. (2001), Climatology of dust aerosol size distribution and optical properties derived from remotely sensed data in the solar spectrum, *J. Geophys. Res.*, *106*, 18,205–18,217.

Tegen, I., and I. Fung (1994), Modeling of mineral dust in the atmosphere—Sources, transport, and optical-thickness, *J. Geophys. Res.*, *99*, 22,897–22,914.

Tegen, I., M. Werner, S. P. Harrison, and K. E. Kohfeld (2004), Relative importance of climate and land use in determining present and future global soil dust emission, *Geophys. Res. Lett.*, *31*, L05105, doi:10.1029/2003GL019216.

Torres, O., et al. (2002), A long-term record of aerosol optical depth from TOMS observations and comparison to AERONET measurements, *J. Atmos. Sci.*, *59*, 398–413.

Welton, E. J., J. R. Campbell, T. A. Berkoff, J. D. Spinhirne, and P. Ginoux (2001), Initial results from the Micropulse Lidar Network (MPLNET), *Eos Trans. AGU*, *82*, Fall Meet. Suppl., Abstract A21A-0023.

————————————

S. Fan and P. Ginoux, NOAA Geophysical Fluids Dynamics Laboratory, Princeton University, Forrestal Campus, Route 1, P.O. Box 308, Princeton, NJ 08542-0308, USA.

Y. J. Kaufman and L. A. Remer, NASA Goddard Space Flight Center, Greenbelt, MD 20771, USA. (kaufman@climate.gsfc.nasa.gov)

I. Koren, National Research Council, Greenbelt, MD 20771, USA.

D. Tanré, Laboratoire d'Optique Atmospherique, CNRS, Université, de Science et Technique de Lille, F-59655 Villeneuve d'Ascq, France.